IOP Publishing Phys. Med. Biol. 65 (2020) 085008 https://doi.org/10.1088/1361-6560/ab7974

Physics in Medicine & Biology

IPEM Institute of Physics and Engineering in Medicine

PAPER

RECEIVED
28 October 2019

REVISED
19 February 2020

ACCEPTED FOR PUBLICATION
24 February 2020

PUBLISHED
20 April 2020

Optimization of irradiation interval for fractionated stereotactic radiosurgery by a cellular automata model with reoxygenation effects

Daisuke Kawahara[1], **Lin Wu**[2] **and Yoichi Watanabe**[2]

[1] Department of Radiation Oncology, Institute of Biomedical & Health Sciences, Hiroshima University, 1-2-3 Kasumi, Minami-ku, Hiroshima City, Hiroshima 734-8551, Japan

[2] Department of Radiation Oncology, University of Minnesota-Twin Cities, 420 Delaware St. SE, MMC494, Minneapolis, MN 55455, United States of America

E-mail: daika99@hiroshima-u.ac.jp

Keywords: automata model, radiation effect, hypoxia, SRS

Abstract

The current study aims to determine the optimal irradiation interval of fractionated stereotactic radiosurgery (SRS) by using an improved cellular automata (CA) model. The tumor growth process was simulated by considering the amount of oxygen and the density of blood vessels, which supplied oxygen and nutrient required for cell growth. Cancer cells died by the mitotic death process due to radiation, which was quantified by the LQ-model, or the apoptosis due to the lack of nutrients. The radiation caused increased permeation of plasma protein through the blood vessel or the breakdown of the vasculature. Consequently, these changes lead to a change in radiation sensitivity of cancer cells and tumor growth rate after irradiation. The optimal model parameters were determined with experimental data of the rat tumor volume. The tumor control probability (TCP) was defined as the ratio of the number of histories in which all cancer cells died after the irradiation to the total number of the histories per simulation. The optimal irradiation interval was defined as the irradiation interval that TCP was the maximum. For one fractionation treatment, the ratio of hypoxic cells to the total number of cancer cells kept decreasing until day 16th after irradiation; whereas the number of surviving cancer cells begun increasing immediately after irradiation. This intricate relationship between the hypoxia (or reoxygenation) and the number of cancer cells lead to an optimal irradiation interval for the second irradiation. The optimal irradiation interval for two-fraction SRS was six days. The optimum intervals for the first-second irradiations and the second-third irradiations were five and two days, respectively, for three fraction SRS. For 4 and 5-fraction treatments, the optimum first-interval was five days, which was similar to three fraction treatment. The remaining intervals should be one day. We showed that the improved CA model could be used to optimize the irradiation interval by explicitly including the reoxygenation after irradiation in the model.

1. Introduction

Technological advancement in stereotactic radiosurgery (SRS) and stereotactic body radiotherapy (SBRT) allows us to deliver radiation in a single large fraction precisely to the tumor-bearing volume (Timmerman *et al* 2010, Kim *et al* 2011, Nagata 2013, Staehler *et al* 2015). Although the radiation damage to cancer cells causes mainly direct cell death, i.e. mitotic catastrophe, recent studies showed that in addition to the direct cell death, indirect cell death through vascular damage occurs when tumors are exposed to high dose hypo-fractionated irradiation (Kocher *et al* 2000, Park *et al* 2012). Kim *et al* described experimental evidence that the indirect cell death due to vascular damage and ensuing immune responses may play crucial roles in the response of a tumor to SRS and SBRT (2015). Meanwhile, Carlson *et al* suggested that tumor hypoxia is a serious problem with daily fractioned SBRT because of a reduction in inter-fractionation reoxygenation

associated with single high dose irradiation (2011). Hypoxia causes the production of the slow-proliferating stem-cell-like phenotype of cells, decreases senescence, creates chaotic and malfunctioning blood vessels, and augments metastasis, which all together further induce therapy resistance (Vaupel *et al* 2001). Assuming that 10%–20% of cancer cells are hypoxic and using the conventional radiobiological model, Brown, *et al* indicated that the radiation doses used in SBRT are insufficient to kill all the clonogenic cells in 1–3 cm diameter tumors (2010).

Mathematical modeling of biological processes is widely used to enhance the quantitative understanding of biomedical phenomena. These models provide quantitative knowledge that can be applied in both experimental and clinical settings. In cancer biology, many mathematical models have been developed (Araujo and McElwain 2004, Cristini *et al* 2009). Von Neumann conceived the idea of cellular automata (CA) (Pesavento 1995). Models based on cellular automata have been widely utilized in studies related to biological systems (Ganguly *et al* 2003, Alber *et al* 2003). Duchting and Vogelsager proposed the application of CA for modeling cancers with radiotherapy effects (Duchting and Vogelsaenger 1985). Richard *et al* developed a simple deterministic model based on a cellular automaton (2009a, 2009b), which is useful to describe the dynamics of a population of proliferating cells. The cellular automata can be used to model the treatment response of tumors and the effects of the oxygen diffusion on the response to radiation therapy. Paul-Gilloteaux *et al* incorporated the blood vessel and oxygen diffusion map into a CA simulation (2017).

In the current study, we built a cellular automata model for simulation of hypo-fractionated radiotherapy or SRS/SBRT. Our model included direct cell death caused by radiation (or mitotic catastrophe) and indirect death by apoptosis. We explicitly incorporated the radiation damage of blood vessels caused by the death of endothelial cells in the model. The damage to blood vessels lead to decreased oxygen supply to the tumor, which in turn affected the radiation sensitivity and the growth rate of cancer cells after irradiation. Furthermore, the decrease of the nutrient supply due to the radiation damage of blood vessels caused death of the cancer cells by indirect death mechanism (or apoptosis). The model contained four populations of cancer cells: proliferating cancer cells, doomed cells, dead cancer cells, and arrested cells. Using the proposed model, we studied the optimized fractionation schedule for SRS/SBRT to maximize the tumor control probability (TCP) by taking advantage of reoxygenation after irradiation.

2. Materials and methods

2.1. Cellular automata model

Automata are commonly placed on a grid structure and updated at discrete time intervals to reflect their new states based on changes in the environment. In the current study, we implemented a two-dimensional (2D) cellular automata model to study the response of a tumor to radiotherapy and the impact of the tumor microenvironment (vascularization, nutrient, and oxygen levels) on the therapeutic response. Every compartment or pixel in the 2D lattice was assigned to one of the following six cell types: healthy cell, cancer cells in four different states (proliferating cancer cell, doomed cell, dead cancer cell, and arrested cell), and blood vessel. The division and multiplication of cancer cells depended on the type of neighbor cells, mechanical pressure, and cellular microenvironment. Arrested cells were created from cancer cells by apoptosis due to the lack of nutrients. Doomed cells were created from proliferating cancer cells by irradiation. The arrested and doomed cancer cells were converted to dead cancer cells at a constant rate. Cellular automata simulation started with four cancer cells at the center of the 2D lattice. The simulation was continued for a certain period before and after irradiation to observe the dynamic changes of the cell population and the spatial distribution. Our simulation was stochastic, so we ran many histories per simulation with fixed model parameter values.

Our simulation used a 2D lattice composed of square pixels of 15 μm $\times$ 15 μm. The volume of the tumor in the 3D space was estimated by taking the 3/2 power of the 2D volume. We used a 2D model to keep the simulation time in a reasonable length for a parametric study (to run many cases by varying model parameters.) The total volume of a tumor before treatment was 0.5–1 cc.

Simulating blood vessels is essential in this work. Helmlinger *et al* reported blood vessel diameters in the range of 10–80 μm and the median radius of 22.5 μm (1997). Thus, in our model, blood vessels were randomly assigned to the lattice by assuming that one blood vessel occupied one pixel. The initial vessel density (i.e. the ratio of the number of blood vessels to the total number of pixels in the 2D lattice) was set at 3.8%. We assumed that the number of blood vessels could increase slowly with a constant growth rate.

2.1.1. Proliferation

There are three factors affecting the proliferation and invasion of cancer cells. Those are the type of neighbor cells, mechanical pressure, and cellular microenvironment, such as the amount of oxygen and nutrient available for cancer cells.

Each cell in a pixel has neighbors. Each cell chooses its next state, based on some predefined rules along with the surrounding microenvironment. The critical part of the implementation of cellular automata is the definition of proper rules so that the model can simulate the natural phenomena appropriately. For a proliferating cancer cell at a pixel, the cell is duplicated to two cancer cells with a probability P_c at each time step. One of those remains at the original location, and the other (or daughter cell) moves to one of the four neighbor pixels, which is occupied by a normal cell.

The mechanical pressure within the tumor is an essential factor in the local invasion. Qi *et al* proposed a modified cellular automata model for cancer growth (1993). To reproduce the Gompertzian-like growth of tumors, they incorporated biologic properties such as the cytotoxic effect of the immune system and the mechanical pressure inside the tumor into the cellular automata model in addition to the proliferation of cancer cells. Following the Qi *et al*, we included the effects of mechanical pressure in our model as follows. Only if the pressure inside the tumor was high enough, the expansion of the tumor was possible. The mechanical pressure was related to the density of cells.

Let N_c, N_d, N_D, and N_a denote the number of cancer cells, doomed cells, dead cancer cells, and arrested cells, respectively. Then, the total number of cancer cells, N, was a sum of these four cancer cell types,

$$N = N_c + N_d + N_D + N_a \tag{1}$$

We defined the average radius of the cancer cell distribution or tumor, R_t, as

$$R_t = \left(\Sigma R_{i,j}\right)/N \tag{2}$$

We assumed that the center of a cell coincided with the center of a pixel in the 2D lattice. The center of the tumor, then, was calculated as the center of mass of all four types of cancer cells. In equation(2), $R_{i,j}$ is the distance of the cell at pixel (i, j) from the center of the tumor.

We introduced the density of cells, ρ, to describe the effect of mechanical pressure on tumor development. It was defined by

$$\rho = N/R_t^2 \tag{3}$$

The cancer cell growth mechanism depends on the magnitude of the density ρ relative to a critical density ρ_c. The relationship between ρ and ρ_c is given as follows (Qi *et al* 1993):

(a) If $\rho \leq \rho_c$, the daughter cell resulting from the proliferation, can only occupy one of the inside nearest neighboring sites originally occupied by normal cells with the same probability.
(b) If $\rho > \rho_c$, the daughter cell can invade any one of the nearest neighboring sites originally occupied by normal cells with the same probability.

Qi *et al* (1993) found the optimum value of ρ_c to be 3.7 through extensive simulation, and we adopted the same value in the current simulation. Since the pixel size was 15 μm × 15 μm, ρ_c could be calculated as $3.7/(0.015 \times 0.015)$ cells mm^{-2} $= 1.6 \times 10^6$ cells cm^{-2} in 2D simulation. The volume of the tumor in the 3D space was estimated by taking the 3/2 power of the 2D volume. Consequently, the ρ_c in the 3D simulation is to be $(1.6 \times 10^6)^{3/2} = 2.0 \times 10^9$ cm^3.

Oxygen and nutrient concentrations affect cancer cell proliferation. The probability of cell proliferation, P_c, is represented by

$$Pc = Po\left(\frac{R_{O_2}}{R_{O_{2max}}} + \frac{R_{nu}}{R_{nu_{max}}}\right) \tag{4}$$

The second factor in equation (4) indicates the effect of oxygen and nutrient. The parameters R_{O_2} and R_{nu} are the local oxygen and nutrient concentrations, respectively. $R_{O_{2max}}$ and $R_{nu_{max}}$ were estimated maximum oxygen and nutrient concentrations. We assumed that $R_{O_{2max}}$ is equal to the normal oxygen level, which is 21% (McKeown 2014). Here, the oxygen concentration is given as the partial oxygen pressure of the standard atmospheric pressure. The maximum R_{nu} is 100%, but it does not exceed 10% under normal circumstances. In equation (4), the unmodulated cell proliferation probability P_0 was calculated from the tumor volume doubling time, T_{cd}, and the time step used for the simulation, Δt, as follows.

$$Po = \frac{1}{2}\mathrm{e}^{\left(In(2)\frac{\Delta t}{T_{cd}}\right)} \tag{5}$$

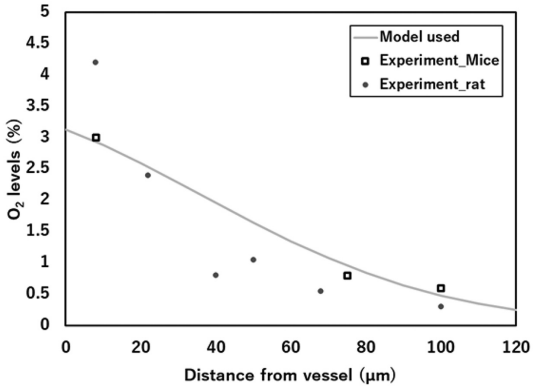

Figure 1. The partial pressure of O_2 (% of atmospheric pressure, pO_2) as a function of the distance from the surface of one vessel wall. The experimental data were taken from Paul-Gilloteaux P *et al* 2017 and Helmlinger G *et al* 1997.

2.1.2. Oxygen and nutrient concentrations

Our model incorporated the oxygen (O_2) diffusion through blood vessels by assuming that the tumor is homeostasis or in a steady-state, leading to no net change of oxygen from cell consumption. The O_2 maps of the 2D lattice were computed at each time step. We calculated the oxygen distribution or map by assuming that the spatial distribution of oxygen concentration per blood vessel follows the Gaussian distribution. Note that the blood vessels are lines running perpendicular to the lattice plane. If the blood vessel is located at a pixel at (0, 0), the amount of oxygen, or the partial oxygen pressure, R_{O2}, at a pixel at (x, y) can be represented by

$$R_{O_2}(x,y) = \frac{1}{2\pi\sigma^2} e^{\frac{-x^2-y^2}{2\sigma^2}} \tag{6}$$

Note that equation (6) is a solution of a diffusion equation with a diffusion coefficient σ. The value σ was determined by fitting experimental data (Helmlinger *et al* 1997, Paul-Gilloteaux *et al* 2017) with equation (6), as shown in figure 1. The estimated value σ was 2.4.

The transport process of nutrients in tissue can be represented by the same diffusion equation as oxygen, but with a diffusion coefficient different from oxygen. Hence, we used equation (6) to estimate the amount of nutrients available by a cell at pixel (x, y). The current study assumed that the oxygen level was in an equilibrium state, where the oxygen supply and consumption were balanced. Thus, the oxygen level changed instantly and achieved a new equilibrium state after the blood vessel or the tumor cell died.

2.1.3. Indirect damage by apoptosis

The number of cancer cells, adjacent to a blood vessel, can impact on the available nutrients (Gerlee and Anderson 2008). In other words, as the number of cancer cells increases, the more nutrients will be required, which leads to nutrient scarcity. The current study assumed that the cancer cell turns to the arrested cell with the apoptosis probability P_{nd} if the nutrient was smaller than the threshold value, R^*_{nu}, of 1%. The repair of the arrested cell was not considered, i.e. the repair probability P_{ar} was set to equal to 0.

2.1.4. Radiation response

The cancer cell is damaged by the irradiation, which causes direct cell death. The killing probability, P_{LQ}, was calculated by using the linear-quadratic (LQ) model: (Fowler 1989)

$$P_{LQ} = 1 - e^{-aD-bD^2} \tag{7}$$

The effective dose, D', is smaller than the physical dose D when the oxygen effect is considered:

$$D' = D/\mathrm{HRF} \tag{8}$$

Here HRF is the hypoxia reduction factor and defined by (Carlson *et al* 2011):

$$\mathrm{HRF} = \frac{mk + R_{O_2}}{k + R_{O_2}} \tag{9}$$

where k is the oxygen partial pressure at which the HRF is half the maximum value, and m is the maximum HRF. The current study used 2.804 for m and 0.1076 for k. These values were taken from the past study in

which the authors estimated the value of m and k parameters by fitting the formula with experiment data (Paul-Gilloteaux *et al* 2017). Thus, when the oxygen effect on the cell-killing capacity is considered, the killing probability P_{LQ} now must be modified by replacing D by the effective dose D' in equation (7), as follows:

$$P_{LQ} = 1 - e^{-aD' - bD'^2} \tag{10}$$

For the current study, we modeled the effects of radiation damage of blood vessels. Potiron *et al* showed that blood vessels become more permeable and increase tumor oxygenation after irradiation by using a Monte Carlo approach with *in vitro* experimental data (Potiron *et al* 2013). The amount of O_2 passing through the endothelial wall is increased by a multiplicative factor L_f if radiation damages a blood vessel cell. The L_f is 1.5 from the measurement data *in vitro* (Paul-Gilloteaux *et al* 2017). We assumed that the blood vessels become more permeable for dose below 6 Gy. At doses above 6 Gy, the radiation induces vessel death, which causes hypoxia, consequently, tumor radio-resistance. This phenomenon is known as the tumor bed effect. By following the work of Paul-Gilloteaux *et al* (2017), we modeled the radiation damage of blood vessel such that the vessel survival probability, P_{dv}, decreases linearly from 1 to 0.2 for the dose between 6 and 30 Gy, and it decreases linearly from 0.2 to 0.0 between 30 Gy and 40 Gy. In short, P_{dv} can be expressed by

$$P_{dv} = \begin{cases} 1.0 & \text{for } 0\text{ Gy} \le D \le 6\text{ Gy} \quad (11a) \\ -0.8/24^{*}\,(D-6) + 1.0 & \text{for } 6\text{ Gy} < D \le 30\text{ Gy} \quad (11b) \\ -0.2/10^{*}\,(D-30) + 0.2 & \text{for } 30\text{ Gy} < D \le 40\text{ Gy} \quad (11c) \\ 0 & \text{for } 40\text{ Gy} < D \quad (11d) \end{cases}$$

Song *et al* showed that cancer cells are hypoxic due to the inadequate blood supply, and they die even without radiation exposure (Song *et al* 2019). The current study assumed the indirect death of cancer cells that occurred by a lack of blood flow, resulting in a decrease in the supply of the nutrient to the cells.

2.1.5. Summary of biologic processes used in cellular automata simulation

We made a model that can accurately predict cell death depending on oxygen and nutrient levels and vessel density. The diagram shown in the flowchart of figure 2 summarizes the biologic processes with transition parameters (probabilities and half-lives) implemented in the current CA model. The biologic processes simulated by the model can be described as follows:

(a) Blood vessels are randomly distributed on the 2D lattice. The oxygen and nutrient distributions are obtained for each blood vessel. Then, the concentrations at each pixel were calculated as a sum of contributions from all blood vessels.
(b) The current study assumed that the mitotic catastrophe is the main mechanism of radiation-induced cell death. This assumption is in good agreement with the general consensus of the occurrence of mitotic catastrophe (Castedo *et al* 2004).
(c) Cancer cells proliferate with probability P_c and by the lattice rules.
(d) A cancer cell, which cannot multiply due to radiation damage, turns to a doomed cell. Here, the doomed cell is the cancer cell, which is damaged by radiation and will die eventually in the future. If the random probability of death P_{d2} was smaller than the killing probability of radiation P_{LQ}, the cancer cell is replaced by a doomed cell.
(e) A cancer cell can turn to an arrested cell by a lack of nutrients. If the nutrient level is smaller than the threshold value, R^{*}_{nu}, the cancer cell is replaced with an arrested cell with the apoptosis probability P_{nd}. An arrested cell turns to a cancer cell if the random probability of death P_{id} is smaller than apoptosis repair probability P_{ar}. The current simulation did not consider the threshold of value of the nutrient level, the apoptosis probability, and repair probability; thus, R^{*}_{nu}, P_{nd}, and P_{ar} were set to 0.
(f) The arrested cell is replaced with a dead cell at a constant rate with the half-life of T_a. The doomed cell is replaced by a dead cell at a constant rate with the half-life of T_d.
(g) There is a balance between the supply and consumption of oxygen by cancer cells in a tumor before irradiation. After irradiation, some cancer cells die and stop consuming the oxygen. This extra amount of oxygen becomes available for the remaining cells (doomed cells and surviving cancer cells). Lambda, Λ, defines the fraction of the oxygen re-distributed to/or shared by surviving cancer cells out of the total amount of extra oxygen being available for cells in the tumor after a single irradiation. $\Lambda = 0$ means no extra oxygen is available to the cancer cells. $\Lambda = 1$ means the whole extra oxygen becomes consumable by the cancer cells. The value depends on many factors, such as the oxygen consumption rate (or the metabolism) of the remaining cells in the tumor, the microenvironment, including the interstitial fluid pressure, and the distance of the cells from blood vessels, which were not included in the current model.

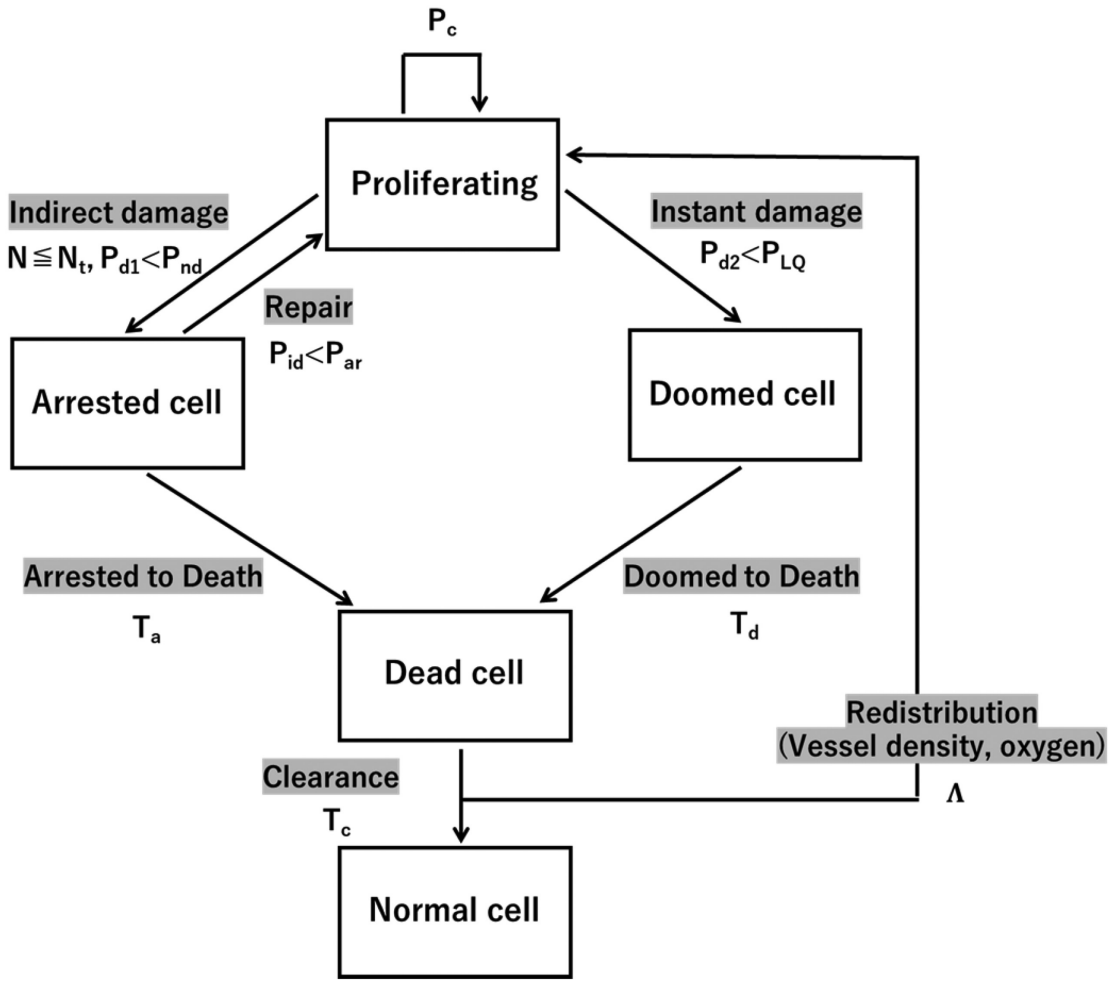

Figure 2. The process of the cellular automata model in the current study.

In this study, we selected a Λ value of 0.3 so that the model could closely simulate the change of oxygen before and after irradiation by including the oxygen redistribution effect on the hypoxia.

(h) The dead cell is dissolved at a constant rate and replaced by a normal cell with the half-life of T_c.

It is noted that our simulation model can easily accommodate non-uniform dose distributions, which are designed to conform to the tumor volume. However, we assumed a uniform dose distribution for all the results presented in the current work. Furthermore, we set the time step of the simulation Δt to one day for all the simulation results presented in this study.

2.2. Model validation and parameter optimization

To validate our CA model, we used the experimental data published by Barendsen and Broerse (1969). They used rhabdomyosarcoma tumors, which were transplanted in rats. Tumors were exposed to the 300 kV x-rays with the radiation dose ranging from 10 Gy to 40 Gy in one fraction. The volume of the tumor before and after irradiation was measured by a caliper.

For the CA simulation, the volume of the tumor was determined by adding the numbers of four types of cancer cells (proliferating cancer cells, doomed cells, dead cancer cells, and arrested cells) at every time step. Since the volume of all cells is the same, the 2D volume of tumor is proportional to the number of cells. Then, the volume of the tumor in the 3D space was estimated by taking the 3/2 power of the 2D volume.

We attempted to match simulation results with Barendsen's experimental data by varying the model parameters. For the simulation, the irradiation was performed on the 20-th day. The α/β value of the LQ model was set to 5 Gy. The model parameter values were used for the subsequent simulations for the irradiation interval optimization study.

2.3. Optimal irradiation interval

Before and after radiation therapy, the oxygen concentration in tumor changes because of the change in oxygen consumption and supply. After irradiation, the tumor may become more hypoxic than before the irradiation; however, the surviving cancer cells eventually gain oxygen due to four mechanisms: (1) reduced O_2 metabolism, (2) improved circulation, (3) shrinkage, and (4) migration (Kalllman 1972). The time scale of these reoxygenation processes after the high dose delivered in a short time is not well characterized. We hypothesized that the oxygen level per cell in surviving cancer cells increases due to the excessive supply caused by the sudden death of oxygen starving cancer cells. Since the oxygen environment rapidly changes with the changes in the number of oxygen-consuming cancer cells after irradiation, we could expect that at a specific time after irradiation, the ratio of hypoxic and anoxic cells take a minimum then it increases again making the tumor hypoxic. Therefore, we think there is an optimum time after the first irradiation at which the second irradiation is the most effective in terms of the cell-killing capacity of the radiation. If there are more than two fractions of irradiation, there may be an optimum time for the third fraction, too. In this work, we studied the optimum time intervals only for two to five fraction treatments.

For the analysis, we used the model parameters obtained in Section 2.2. The tumor was irradiated with a uniform dose. The first irradiation was delivered on the 100th day after the start of the simulation. For the single fraction treatment, we used 20 Gy. For the 2 to 5 fraction treatment, the dose per fraction, d', was calculated by using the biological equivalent dose (BED), and it is given by.

$$d' = \frac{-\alpha/\beta + \sqrt{\alpha/\beta^2 + 4\frac{\alpha/\beta}{n'^2} \cdot BED_{1fr}}}{2} \tag{12}$$

where $\alpha/\beta = 5$, n' is the number of the fraction. The d' is the dose per fraction for two to five fraction treatments. BED_{1fr} is the biologically equivalent dose with dose d given in one fraction. BED_{1fr} is calculated as follows:

$$BED_{1fr} = d\left(1 + \frac{d}{\alpha/\beta}\right) \tag{13}$$

where d = 20 Gy.

The tumor control probability (TCP) was defined as the ratio of the number of histories in which all cancer cells died after the irradiation to the total number of the histories per simulation. The optimal irradiation interval was defined as the irradiation interval that TCP was the maximum. We evaluated the following quantities.

- Tumor volume
- Total volumes of the proliferating cancer cells, doomed cells, dead cancer cells, and arrested cells after irradiation
- The ratio of hypoxic cancer cells to the total number of cancer cells:

We used three levels of hypoxia: 0.2% oxygen level, which was used for hypoxia in Paul-Gilloteaux et al (2017), 0.4% oxygen level, which is radiobiological hypoxia (McKeown 2014).

- Vessel volume and vessel density inside the tumor. The vessel density is the ratio of the vessel volume to the total volume of the cancer.
- The second through fifth treatment days to achieve the maximum TCP for fractionated treatment.

3. Results

3.1. The optimal model parameters

Figure 3 shows the total tumor volumes, which were the sum of cancer cells, doomed cells, dead cells, and arrested cells, for the Barendsen's experiments. Both the experimental data (symbols) and the CA simulation results (lines) are plotted. In the figure, the volume was normalized to the volume of day 20, on which the tumor was irradiated. The relative tumor volume of the simulation agreed with the measurement within standard deviations for 0, 10, 20, 30, and 40 Gy cases. Some of the fitting parameters were listed in table 1.

3.2. Characteristics of single fraction

Figure 4 (a) shows the volume of the tumor, 'Total', including all four types of cells (proliferating cancer cells, doomed cells, dead cells, and arrested cells), and the volume of proliferating cancer cells, 'Tumor', as a function of time. A single dose of 13.5 Gy was given to the tumor on day 100. Both volumes were normalized

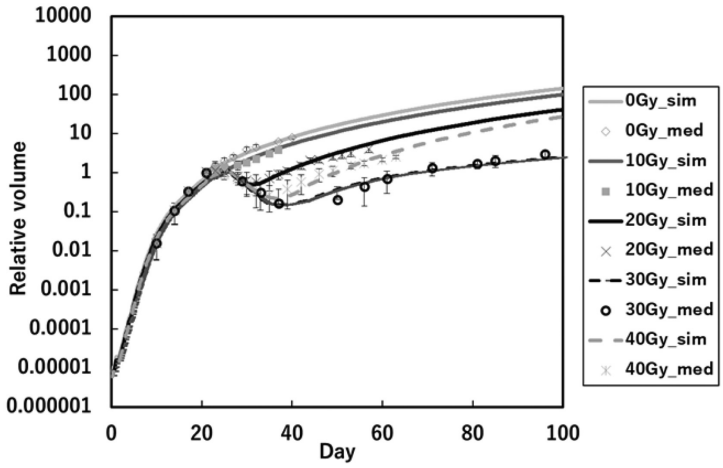

Figure 3. The relative tumor volume of the measurement and the simulation. For each simulation and calculation, the total tumor volume was normalized on day 20, on which the tumor was irradiated.

Table 1. The values of model parameters obtained by fitting the simulation with the experimental data. Here, T_{cd} is the doubling time of the tumor, T_d is the time of the doomed cell to die, T_c is the time of the dead cell to clear, and λ is the ratio of the oxygen redistribution from dead cells to surviving cells.

Parameters	Fitting value
T_{cd} (days)	0.6
α/β	5
T_d (days)	5
T_c (days)	6
Vessel density (g cm^{-3})	0.038
λ	0.3

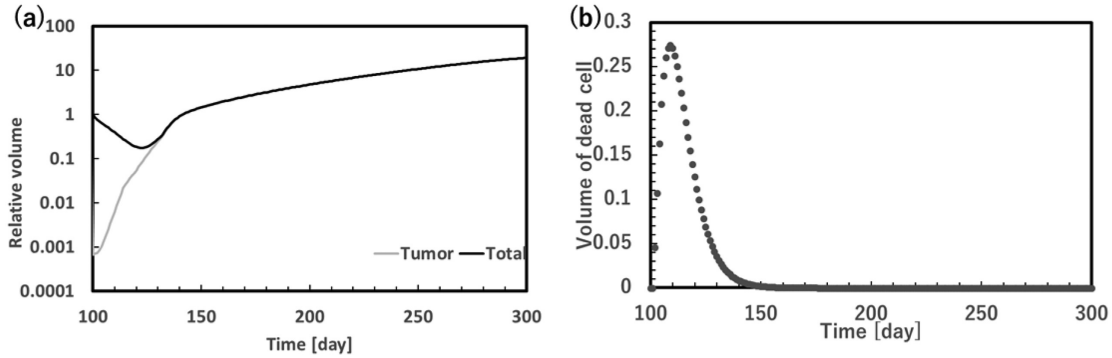

Figure 4. (a) Relative volumes of the entire tumor ('Total') and proliferating cancer cells ('Tumor') vs. the time in days. The volumes were normalized to the total tumor volume at the time of the irradiation. (b) The volume of the dead cells vs. the time in days. For (a) and (b), the tumor was irradiated with a single dose of 13.5 Gy on day 100.

to the total tumor volume on day 100. The number of proliferating cancer cells decreased instantly after irradiation, then it rapidly increased. On the other hand, the total tumor volume gradually decreased until day 26; then, it started growing.

Figure 4(b) shows the volume of dead cells as a function of time. The volume of dead cells kept increasing until day 110, after which it decreased. The time scale was governed by the two time constants: the transition time from the doomed to dead cells, T_d (=5 d), and the clearance time of the dead cells, T_c (=6 d).

Figure 5(a) shows the total volume of blood vessels inside the tumor as the function of time in days. To calculate the volume, only blood vessels, whose neighboring cells were one of the cancer cells (proliferating, doomed, dead, and arrested), were considered to be the inside of the tumor. The volume of blood vessels increased as the tumor grew before irradiation. The volume suddenly decreased at the time of irradiation, i.e. on day 100, due to radiation-induced death. Then, the volume stayed constant for about 25 d because the blood vessel had a high chance of having non-healthy cells such as proliferating cancer, doomed,

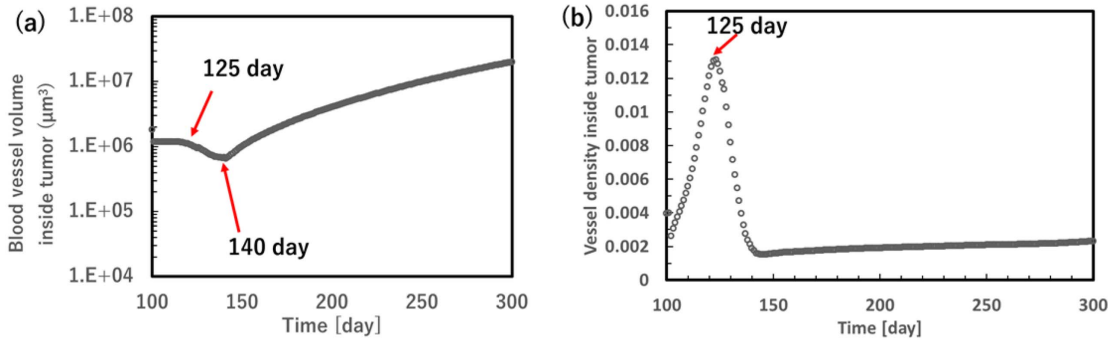

Figure 5. (a) The volume of blood vessels vs. the time in days. (b) The vessel density vs. the time in days. The vessel density is the ratio of the vessel volume to the total volume of the cancer.A single dose of 13.5 Gy was given to the tumor on day 100.

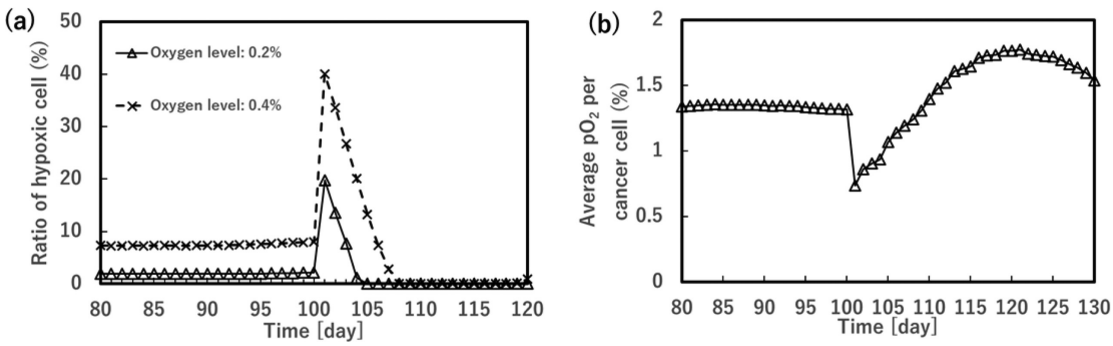

Figure 6. (a) The fraction of the number of hypoxic cells at 0.2% and 0.4% oxygen levels to the total cancer cells vs. the time in days. (b) The ratio [%] of the average partial oxygen pressure, pO_2, per cancer cell vs. the time in days. A single dose of 13.5 Gy was given to the tumor on day 100.

dead, or arrested cells in the neighborhood. Between day 125 to day 140, the volume decreased because most of the doomed and dead cells disappeared during this time, as shown in figure 4(b), resulting in a less amount of blood vessels inside the tumor. After day 140, the number started increasing again because of the increase of the tumor size and the formation of new blood vessels.

Figure 5(b) shows the blood vessel density inside the tumor as the function of time in days. As discussed above, the number of blood vessels in the tumor was almost constant from the time of irradiation (day 100) to day 125. But the actual tumor size decreased, as seen in figure 4(a). This resulted in a rapid increase in the density, reaching the maximum at day 125. After that, the density decreased due to the decreasing number of blood vessels inside the tumor, as indicated in figure 5(a).

Figure 6 (a) shows the relative number of hypoxic cells or the ratio of the number of hypoxic proliferating cancer cells to all proliferating cancer cells after irradiation with 13.5 Gy on day 100. For the analysis, we considered that a cancer cell with oxygen concentration at 0.2% and 0.4% levels as the hypoxia threshold. The ratio increased immediately after irradiation for all hypoxia thresholds. The peak ratios were 0.20 and 0.41 for 0.2 and 0.4% hypoxia threshold, respectively, on day 101. Then, it kept decreasing until days 105 and 108 for the two thresholds because the doomed cells continuously died and stopped consuming the oxygen. The redistribution of the available oxygen from the dead cancer cells to the surviving proliferating cancer cells, whose number was much smaller than pre-irradiation, caused the increase of average oxygen level (pO_2) per cancer cell, as seen in figure 6(b). This led to a decrease in the ratio of hypoxic cancer cells, as seen in figure 6(a). The decrease in the number of hypoxic cells indicates the re-oxygenation of the tumor.

Figure 7 shows the average HRF values in cancer cells from day 100 to day 120. The HRF decreased until day 114, and then it increased again. HRF decreased because of the increase of the average oxygen concentration per cell, which is seen in figure 6(b).

Figure 8 shows the relative numbers of hypoxic cells at 0.4% oxygen level, which is radiobiological hypoxia after irradiation for three different doses of 5, 10, and 15 Gy. The trend is similar to that seen in figure 6(a) with 13.5 Gy. The cells became hypoxic after irradiation, but the ratio of hypoxic cells decreased to a very low level within about seven days after irradiation. Also, we can observe the level of hypoxia is higher for larger doses because there is more damage to the blood vessels with increasing dose.

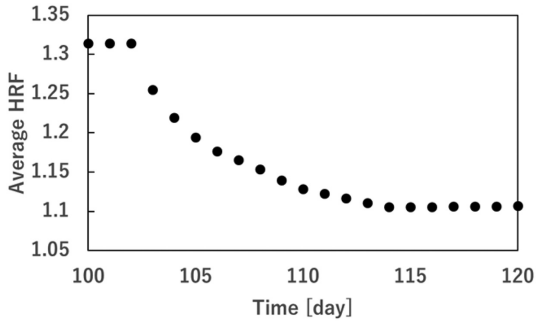

Figure 7. The average HRF values in cancer cells on day 100 to day 120. A single dose of 13.5 Gy was given to the tumor on day 100.

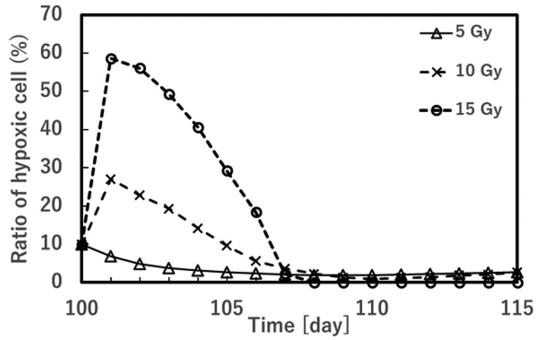

Figure 8. The fraction of the number of hypoxic cells to the number of all cancer cells vs. the time in days. The tumor was irradiated with 5, 10, and 15 Gy on day 100.

3.3. The optimal interval of fractionated treatment

We calculated the dose per fraction for 2- to 5-fraction treatments, which gave the same treatment effect, or BED, as the one-fraction of 20 Gy treatment by using equation (12) and (13). The doses per fraction were 13.5 Gy, 10.6 Gy, 9.0 Gy, and 7.8 Gy for 2-, 3-, 4-, and 5-fraction treatments, respectively. Figure 9 shows that TCP calculated on the 100th day after the first irradiation as the function of the interval between the first and second fraction for the two fraction treatment. The maximum TCP was achieved for a six-day interval, suggesting that the optimal irradiation interval for two fraction treatment was six days. Table 2 shows the TCP as the function of the intervals between the first and second fraction and between the second and third fractions for the three fraction treatment with 10.6 Gy per fraction. The optimal irradiation interval was five days for the first interval and two days for the second interval. Table 3 shows the TCP for 4-fraction treatment with 9.0 Gy per fraction. The optimal irradiation interval was five days for the first interval, one day for the second interval, and one day for the third interval. Table 4 shows the TCP for 5-fraction treatment with 7.8 Gy per fraction. The optimal irradiation interval was five days for the first interval, one day for the second interval, one day for the third interval, and one day for the fourth interval. The daily fraction scheme resulted in the lowest TCP for 2 to 5 fraction treatments

4. Discussion

A previous study introduced a concept of doomed cells, which are cancer cells damaged by radiation but do not die instantly after irradiation (Watanabe *et al* 2016). However, the study was limited to a point kinetic model in which either spatial variation of cell populations or the effects of microenvironment such as oxygen and nutrient were not considered. In the current study, we created a two-dimensional cellular automata model by including four cancer cell populations (proliferating cancer cells, doomed cells, dead cancer cells, and arrested cells) and blood vessels. The inclusion of blood vessels explicitly in the model allowed us to study the effects of oxygen and nutrient on the tumor growth and the radiation response.

Our model could mimic the experimental data very well with a proper selection of model parameters. The proliferating cancer cell population decreases after irradiation because they initially become doomed cells due to damage in DNA. However, the number of cancer cells in the doomed cell population gradually decreased as cell death progresses. Consequently, the simulation results showed that the total tumor volume

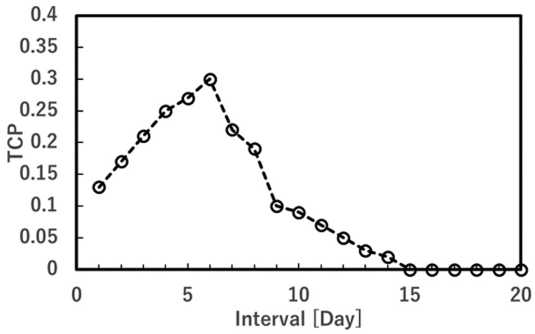

Figure 9. TCP vs. the interval between two fractions of 13.5 Gy each. The first irradiation was made on day 100.

Table 2. TCP vs. the intervals between the first and second irradiation (First interval) and between the second and third irradiation (Second interval) for three fraction treatment with fraction dose of 10.5 Gy.

		First interval						
		2 d	3 d	4 d	5 d	6 d	7 d	8 d
Second interval	1 d	0.1	0.14	0.38	0.34	0.31	0.28	0.24
	2 d	0.12	0.21	0.3	0.38	0.32	0.22	0.21
	3 d	0.18	0.17	0.16	0.3	0.25	0.16	0.14
	4 d	0.25	0.16	0.1	0.18	0.16	0.09	0.07
	5 d	0.15	0.12	0.09	0.15	0.09	0.04	0.02
	6 d	0.1	0.085	0.07	0.06	0.03	0	0

Table 3. TCP for 4-fraction SRS (9 Gy/fraction), intervals between fractions in days.

	1	1	1	1	← 3rd to 4th
1st to 2nd	1	2	3	4	← 2nd to 3rd
1	0.18	0.22	0.19	0.47	
2	0.25	0.21	0.37	0.39	
3	0.34	0.39	0.38	0.38	
4	0.44	0.41	0.29	0.27	
5	0.56	0.34	0.27	0.25	
6	0.48	0.45	0.36	0.23	
7	0.44	0.36	0.34	0.28	
8	0.40	0.36	0.26	0.05	

kept decreasing for 22 d after irradiation after 13.5 Gy with one fraction. Eventually, the tumor volume started increasing because of the proliferation of the surviving cancer cells.

The cancer cells in a hypoxic environment are more resistant to radiation damage than oxic cells, and the degree of hypoxia strongly depends on the number of blood vessels and the amount of blood flow in a tumor (Hall and Giaccia 2011). Horsman *et al* found that tumor blood vessels are often intermittently closed and open, and thus, cancer cells adjacent to the intermittently closed vessels are hypoxic (Horsman *et al* 1995). Song *et al* reported that 10 Gy irradiation increased the carbonic anhydrase 9 (CA9), which is the indicator of tumor hypoxia, for several days after irradiation in HT-1080 human prostate cancer xenografts in nude mice (Song *et al* 2019). Furthermore, in the same paper, the authors showed that high-dose irradiation significantly increased HIF-1α (hypoxia-inducible factor-1α) and CA9 in FSaII sarcoma of mice. Maeda *et al* also showed that high-dose irradiation caused vascular dysfunction, increased tumor hypoxia, and increased HIF-1α (Maeda *et al* 2017). Moreover, Goda *et al* observed in two murine tumor models that after irradiation with a single high-dose, the tumor perfusion decreased, and tumor oxygen pressure (pO_2) also decreased in parallel (Goda *et al* 1996). Kioi *et al* reported that the blood flow decreased but recovered three weeks after irradiation for glioblastoma in mice (Kioi *et al* 2010).

The current study is consistent with these past studies in terms of the temporal changes of vessel volume and vessel density, which cause increased tumor hypoxia, after irradiation. Our study showed that the number of blood vessels decreased after irradiation due to the radiation damage, but the vessel density increased after irradiation because the decrease of the tumor size. The density started decreasing on the 25th day after irradiation, although the day depends on the pattern of tumor volume change. Furthermore, we

Table 4. TCP for 5-fraction SRS (7.8 Gy/fraction × 5), intervals between fractions in days.

	(a) Intervals between 3rd to 4th and 4th to 5th are fixed to one day					
	1	1	1	1	1	←4th to 5th
	1	1	1	1	1	←3rd to 4th
1st to 2nd	1	2	3	4	5	← 2nd to 3rd
1	0.14	0.37	0.41	0.47	0.42	
2	0.35	0.41	0.48	0.49	0.39	
3	0.42	0.42	0.43	0.34	0.30	
4	0.51	0.50	0.43	0.38	0.34	
5	0.58	0.48	0.46	0.36	0.24	
6	0.56	0.42	0.34	0.21	0.20	
7	0.38	0.42	0.24	0.12	0.10	
8	0.24	0.36	0.34	0.11	0.02	
	(b) Intervals between 2nd to 3rd and 4th to 5th are fixed to one day					
	1	1	1	1	1	←4th to 5th
	1	2	3	4	5	← 3rd to 4th
1st to 2nd	1	1	1	1	1	← 2nd to 3rd
1	0.14	0.23	0.22	0.28	0.35	
2	0.35	0.39	0.46	0.34	0.21	
3	0.42	0.34	0.23	0.21	0.19	
4	0.51	0.45	0.38	0.32	0.27	
5	0.58	0.48	0.38	0.30	0.22	
6	0.56	0.38	0.28	0.21	0.12	
7	0.38	0.28	0.34	0.25	0.16	
8	0.24	0.31	0.19	0.16	0.13	

demonstrated an increase in oxygen level and a decrease in the HRF in the cancer cells after irradiation. Our simulation results showed that the proportion of hypoxic cells among the surviving cancer cells decreased up to 7 d after single high-dose irradiation. The result is consistent with Song *et al*, who reported that hypoxic cell fraction decreases and takes its minimum on 5th to 10th days after irradiation depending on the radiation dose (Song *et al* 2019).

The optimal interval of fractionated SRS, which maximizes the tumor control probability (TCP), could be determined by taking advantage of the timing of the reoxygenation after irradiation. In the current study, the optimal irradiation interval for two-fraction treatment with 13.5 Gy per fraction was six days. The optimum interval does not match the day when the reoxygenation is maximum after irradiation because the optimum interval is determined by an intricate balance between the number of hypoxic cells and the proliferation of surviving cancer cells. The increase of the radiation damage due to the decrease of the hypoxic cells is dominant until the sixth day. After that, the enhanced radiation damage is compromised by the increased number of proliferating cancer cells, resulting in a less effect of reoxygenation-aided cell kill capacity on the final tumor size.

For three-fraction treatment with 10.5 Gy per fraction, the first optimum interval was five days. Furthermore, the second irradiation interval was only two days. Since less number of cancer cells are alive after the first irradiation, the reoxygenation effect of oxygen redistribution is smaller. This causes the cancer cells to become hypoxic again quicker, resulting in a short optimum interval between the second and the third fractions.

For 4-fraction treatment with 9.0 Gy per fraction, the optimum first-interval was five days, which was similar to three fraction treatment. The second interval and third interval were one day, and the total treatment time was equal to the three-fraction treatment. Since less number of cancer cells are alive after the first irradiation, the reoxygenation effect is smaller. This causes the cancer cells to become hypoxic again faster, resulting in a short optimum interval between the second and the third fractions. After the third fraction, the cancer cell becomes hypoxic again more quickly since the reoxygenation effect is much smaller, resulting in a short optimum interval between the third and the fourth fractions.

For 5-fraction treatment with 7.8 Gy per fraction, we observed the same trend as that of the 4-fraction treatment. The optimum first-interval was five days. The remaining intervals should be one day. However, it is noteworthy that two fractionation schedules with the first, second, and third intervals of 2, 4, 1 d, and 2, 1, 3 d resulted in similar TCPs.

For 2 to 5 fraction treatment, a daily fractionation scheme is not recommended since the TCP is the lowest. Fractionations with constant intervals would not be good. The current results indicated an optimal fractionation scheme with 5 or 6 d for 1st to 2nd fraction and one-day interval after that. The first two-thirds of dose should be delivered within 7 d to maximize the treatment effect regardless of the number of fractions since the 6 or 7 d time period corresponds to the time of reoxygenation.

The current study showed that there is an optimal irradiation interval for fractionated SRS/SBRT, and the interval length depends on the dose per fraction. The results were obtained by simulation with biologic parameters optimized for animal experiments; therefore, more study with model parameters relevant to humans must be performed in the future to make a definitive recommendation on the optimal fractionation intervals. Nevertheless, we think that in the clinical setting, a first-interval of at least more than one day but less than a week could maximize the treatment outcome by exploiting the reoxygenation effect in fractionated SRS and SBRT.

5. Conclusions

A new CA model could fit the experimental rat data with the rat tumor model very well. The CA simulation could be used to optimize the irradiation interval by taking advantage of reoxygenation for the best outcome of the therapy. We found that the optimum interval for two fraction treatment (13.5 Gy per fraction) was six days. The optimum scheduling of fractionated treatment was determined by an intricate balance of enhanced radiation damage due to reoxygenation and the repopulation of proliferating cancer cells. Hence, a proper selection of simulation parameters is required to enhance the reliability of the prediction results for clinical applications.

Acknowledgments

The authors wish to acknowledge Prof. Chang W Song, University of Minnesota, for his help in interpreting the significance of the results of this study. The part of the work was previously published as an electronic poster at the annual meeting of the American Association of Physicists in Medicine, San Antonio, Texas, USA, 13–18 July 2019.

Appendix: Notations

Symbol	Meaning
T_{cd} [days]	Tumor volume doubling time
T_a [days]	Half-life of apoptotic cell death
T_d [days]	Half-life of doomed cell death
T_c [days]	Half-life of dead cell clearance
Λ	The ratio of oxygen redistribution from dead cells to surviving cells
P_c	Probability of cancer cell proliferation
P_0	Unmodulated probability of cancer cell proliferation
P_{LQ}	Probability of cancer cell death by radiation
P_{nd}	Probability of cancer cell death by apoptosis due to the lack of nutrient
P_{ar}	Probability of repair of arrested cell
P_{dv}	Probability of blood vessel cell death
R^*_{nu}	The nutrient threshold for apoptotic cell death
R^*_{O2}	Threshold oxygen pressure for hypoxia
ρ_c	Critical density
R_{O2}	Oxygen content in a cell, % of standard atmospheric pressure
R_{nu}	Nutrient concentration in a cell, % of the maximum possible amount
σ [cm]	The spread of Gaussian distribution of oxygen in tissue
d [Gy]	Dose per fraction
D [Gy]	Radiation dose
D' [Gy]	Effective dose due to hypoxia and the lack of nutrient
L_f	Oxygen leakage factor of damaged blood vessel
HRF	Hypoxia reduction factor
TCP	Tumor control probability
BED	Biologically effective dose
Δt [day]	Timestep of CA simulation

References

Alber M S *et al* 2003 On cellular automaton approaches to modeling biological cells *Mathematical Systems Theory in Biology, Communications, Computation, and Finance* ed J Rosenthal and D S Gilliam (New York, NY: Springer) pp 1–39

Araujo R P and McElwain D L 2004 A history of the study of solid tumour growth: the contribution of mathematical modelling *Bull. Math. Biol.* **66** 1039–91

Barendsen G W and Broerse J J 1969 Experimental radiotherapy of a rat rhabdomyosarcoma with 15 MeV neutrons and 300 kV x-rays. I. Effects of single exposures *Eur. J. Cancer* **5** 373–91

Brown J M, Diehn M and Loo B W Jr. 2010 Stereotactic ablative radiotherapy should be combined with a hypoxic cell radiosensitizer *Int. J. Radiat. Oncol. Biol. Phys.* **78** 323–7

Carlson D J *et al* 2011 Hypofractionation results in reduced tumor cell kill compared to conventional fractionation for tumors with regions of hypoxia *Int. J. Radiat. Oncol. Biol. Phys.* **79** 1188–95

Castedo M *et al* 2004 Cell death by mitotic catastrophe: a molecular definition *Oncogene* Apr 12 **23** 2825–37

Cristini V *et al* 2009 Nonlinear simulations of solid tumor growth using a mixture model: invasion and branching *J. Math. Biol.* **58** 723–63

Duchting W and Vogelsaenger T 1985 Recent progress in modelling and simulation of three-dimensional tumor growth and treatment *Biosystems* **18** 79–91

Fowler J F 1989 The linear-quadratic formula and progress in fractionated radiotherapy *Br. J. Radiol.* **62** 679–94

Ganguly N *et al* 2003 A survey on cellular automata, centre for high-performance computing, Dresden University of Technology Technical Report 9.

Gerlee P and Anderson A R 2008 A hybrid cellular automaton model of clonal evolution in cancer: the emergence of the glycolytic phenotype *J. Theor. Biol.* **250** 705–22

Goda F *et al* 1996 The relationship between partial pressure of oxygen and perfusion in two murine tumors after X-ray irradiation: a combined gadopentetate dimeglumine dynamic magnetic resonance imaging and in vivo electron paramagnetic resonance oximetry study *Cancer Res.* **56** 3344–9

Hall E J and Giaccia A J 2011 *Radiobiology for the Radiologist* 7th ed edn (Philadelphia, PA: Lippincott Williams&Wilkins)

Helmlinger G *et al* 1997 Interstitial pH and pO2 gradients in solid tumors in vivo: high-resolution measurements reveal a lack of correlation *Nat. Med.* **3** 177–82

Horsman M R, Grau C and Overgaard J 1995 Reoxygenation in a C3H mouse mammary carcinoma. The importance of chronic rather than acute hypoxia *Acta Oncol.* **34** 325–8

Kallman R F 1972 The phenomenon of reoxygenation and its implications for fractionated radiotherapy *Radiology* **105** 135–42

Kim H A, Rhim T and Lee M 2011 *R*egulatory systems for hypoxia-inducible gene expression in ischemic heart disease gene therapy *Adv. Drug Deliv. Rev.* **63** 678–87

Kim M S *et al* 2015 Radiobiological mechanisms of stereotactic body radiation therapy and stereotactic radiation surgery *Radiat. Oncol. J.* **33** 265–75

Kioi M *et al* 2010 Inhibition of vasculogenesis, but not angiogenesis, prevents the recurrence of glioblastoma after irradiation in mice *J. Clin. Invest.* **120** 694–705

Kocher M *et al* 2000 Computer simulation of cytotoxic and vascular effects of radiosurgery in solid and necrotic brain metastases *Radiother. Oncol.* **54** 149–56

Maeda A *et al* 2017 In vivo imaging reveals significant tumor vascular dysfunction and increased tumor hypoxia-inducible factor-1alpha expression induced by high single-dose irradiation in a pancreatic tumor model *Int. J. Radiat. Oncol. Biol. Phys.* **97** 184–94

McKeown S R 2014 Defining normoxia, physoxia and hypoxia in tumours—implications for treatment response *Br. J. Radiol. March* **87** 20130676

Nagata Y 2013 Stereotactic body radiotherapy for early stage lung cancer *Cancer Res. Treat.* **45** 155–61

Park H J *et al* 2012 Radiation-induced vascular damage in tumors: implications of vascular damage in ablative hypofractionated radiotherapy (SBRT and SRS) *Radiat. Res.* **177** 311–27

Paul-Gilloteaux P *et al* 2017 Optimizing radiotherapy protocols using computer automata to model tumour cell death as a function of oxygen diffusion processes *Sci. Rep.* **7** 2280

Pesavento U 1995 An implementation of von Neumann's self-reproducing machine *Artif. Life* **2** 337–54

Potiron V A *et al* 2013 Improved functionality of the vasculature during conventionally fractionated radiation therapy of prostate cancer *PLoS ONE* **8** e84076

Qi A S *et al* 1993 A cellular automaton model of cancerous growth *J. Theor. Biol.* **161** 1–12

Richard M *et al* 2009a Cellular automaton model of cell response to targeted radiation *Appl. Radiat. Isot.* **67** 443–6

Richard M *et al* 2009b A computer model of the Bystander effect: effects of individual behaviours on the population response *Appl. Radiat. Isot.* **67** 440–2

Song C W *et al* 2019 Reoxygenation and repopulation of tumor cells after ablative hypofractionated radiotherapy (SBRT and SRS) in murine tumors *Radiat. Res.* **192** 159–68

Staehler M *et al* 2015 Single fraction radiosurgery for the treatment of renal tumors *J. Urol.* **193** 771–5

Timmerman R *et al* 2010 Stereotactic body radiation therapy for inoperable early stage lung cancer *JAMA* **303** 1070–6

Vaupel P, Kelleher D K and Hockel M 2001 Oxygen status of malignant tumors: pathogenesis of hypoxia and significance for tumor therapy *Semin. Oncol.* **28** 29–35

Watanabe Y *et al* 2016 A mathematical model of tumor growth and its response to single irradiation *Theory Biol. Med. Model.* **13** 6